Bulk Wafer Defects Observable in Vision Chips

Annika Rantzer
Integrated Vision Products AB, Linköping, Sweden and Electronic Devices, Linköpings universitet, Linköping, Sweden
annika.rantzer@ivp.se

Christer Svensson
Electronic Devices, Dept. of Electrical Engineering, Linköpings universitet, Linköping, Sweden
chs@isy.liu.se

Abstract

*Concentric intensity stripes were observed in the images of a 512*512 pixel CMOS camera chip. By measuring wavelength dependence and intensity dependence of the stripes, and analyzing the processed wafers structurally, it was concluded that the observed patterns originate from crystal defects in the bulk of the wafer underneath the epitaxial layer.*

1. Introduction

Images captured by CMOS vision chips from one particular batch showed ring formed stripes with varying response when illuminated by a uniform white light source. The vision chips were fabricated on epitaxial wafers. It was found that the phenomenon was associated to particular wafers, on which all sensors showed a similar pattern. If a CMOS sensor chip from such a wafer was illuminated, the digitized image captured showed rounded stripes with gray values deviating from the major part of the image. When these chips were traced back to the exact position on the wafer, it was found that the stripes formed round circles following the shape of the wafer. One wafer with some of the circuits is shown in Fig 1. The ring pattern was not visible in dark images.

In an earlier investigation similar effects on CCD-chips produced on non-epi wafers were found [1]. Bulk defects and dopant striation caused by the crystal pulling process were discussed as reasons for the concentric intensity variations of the images obtained. Crystal defects, such as stacking faults, arising from precipitation of oxygen, decorated with impurities can serve as recombination or generation centers [2-4]. Thus, the photo current of the pixels could be reduced when a high density of defects is present underneath the pixels.

2. Sensor measurements

The sensor resolution of this chip is 512x512 pixels and the pixel pitch is 18 µm. All measurements have been performed using an on-chip 8-bit analog to digital (AD)-converter. The range is 0-255 AD units where 255 is the brightest value.

The wavelength and intensity dependence was measured by capturing several images, each illuminated by different wavelengths and intensities.

A mean value of the pixel AD-units in an area of several hundred pixels, in the dark and bright areas respectively, was calculated. The difference between these mean values is given by

$$contrast = \frac{1}{N}\sum_{N} bright\_pixels - \frac{1}{M}\sum_{M} dark\_pixels$$

The contrast is a measure of the deviation of the response in the stripes.

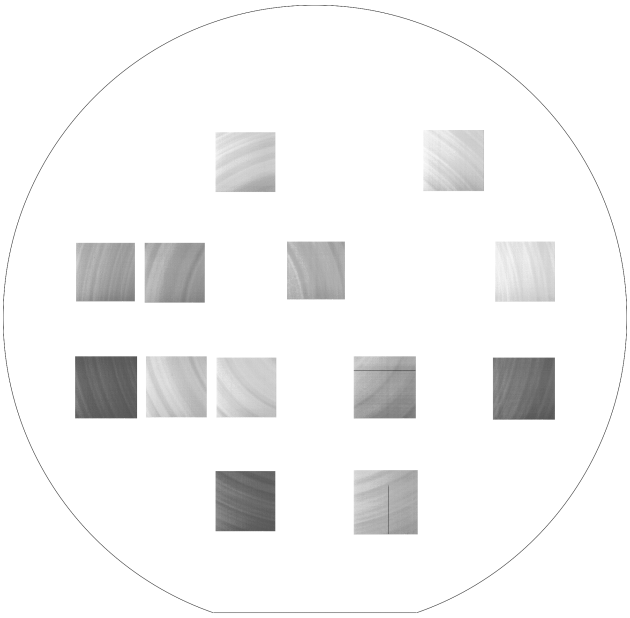

Figure 1. Gray images from circuits traced back to position on wafer. The contrast is enhanced to improve print quality. On the second row there is one circuit that is probably misplaced on the wafer during mounting.

3. Analysis

3.1. Wavelength dependence

The dependence of the stripe-pattern on illumination wavelength was investigated. The measurement was performed at SP, Swedish National Testing and Research Institute, using a spectral lamp. The sensor was irradiated at wavelengths between 650-1100 nm with a 50 nm separation. The bandwidth of the light was 5 nm. An image saved for a wavelength of 950 nm is shown in Fig. 2. The side length of the picture is 9.2 mm (18µm x 512 pixels).

The calculated contrast value was normalized for intensity variations in the illumination source, since it is found that the ring effect is stronger for higher intensity. The resulting graph is shown in Fig. 3. Two different bright/dark stripe combinations were analyzed. It is shown that the rings start to appear at a wavelength of about 750 nm. The contrast value increases then with the wavelength from 2-3% of the AD-unit range to about 10%.

3.2. Intensity dependence

The dependence of the intensity was measured by irradiating the sensor with a white light source with an integrating sphere (OL-452, Optronic Laboratories) to provide spatially uniform illumination. The spectral content of the lamp light ranges from 350 nm to above 1100 nm, with a broad top close to 870 nm. By changing the aperture of the entrance of the light to the integrating sphere, the intensity was linearly increased. The integration time of the sensor was constant.

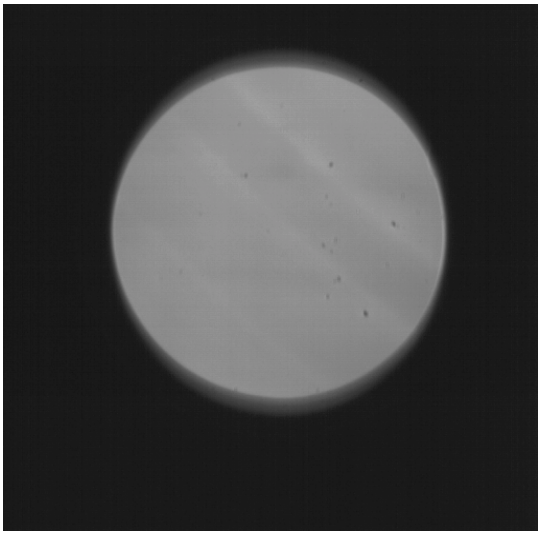

Figure 2. Image saved when irradiating the sensor with 950 nm light. The ring pattern is seen as diagonal brighter stripes. The dark spots seen in the image is dust on the sensor surface.

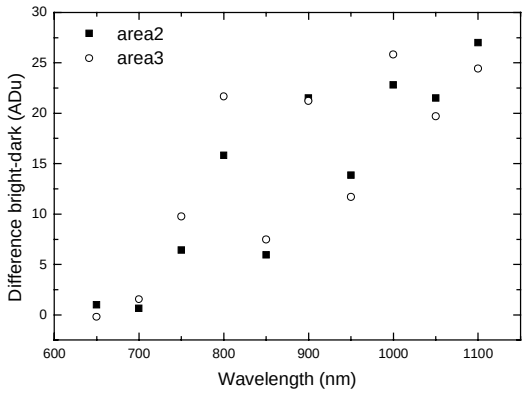

Figure 3. Contrast as difference between dark and bright stripes in AD units when irradiated with different wavelengths.

One of the saved images is shown in Fig. 4. As seen in Fig. 5 the calculated contrast value increases with intensity, and is zero at darkness.

3.3 Spatial distribution

The images in Fig. 2 and Fig. 4, respectively, have a side length of 9.2 mm (18µm x 512 pixels). By measuring the width of the brighter stripes it is possible to compare the spatial spread. From Fig. 4 it can be found that the brighter stripes have a spatial spread of 200-450 µm at a distance of 2-5 mm apart.

Figure 4. One image saved during intensity dependence measurement. The intensity here was 2 W/m^2 (at the output of the sphere).

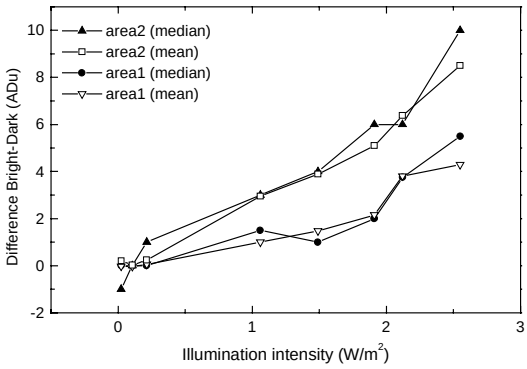

Figure 5. Contrast dependence on intensity

3.4 Resistance measurement

A spreading resistance measurement was done to analyze the dopant concentration below the n-well junctions. A die from an assembled part showing the ring pattern was grounded with a flat bevel angle. There was no concentric ring structure found in the epi-layer at a depth below the n-well junctions and above the highly doped bulk material.

3.5 Structural analysis

An in-depth analysis of the structure of the processed silicon was performed on one chip that showed stripes when operating. A preferential etch experiment using the Yang-etchant [5] was performed. In Fig 6 a photograph after 12.5 min total etching time is shown. After this etching time, 20 µm of silicon was removed. The surface of the die shows concentric grooves with a spacing of 100 to 200 µm. After prolonged etching (22.5 min), crystal defects with a concentric ring structure were found. In Fig 7 the defects are seen as small dots with different density. The depth is around 50 µm below the surface of the chip. In Fig. 8, a photograph of a close-up view of the defect distribution is shown. The dog-bone structures were identified as etching patterns of stacking faults in the crystal. In Fig. 9 a cross-section of a wafer is shown. It is seen that the defect density start about 20 µm below the wafer surface. At the surface of the wafer, a defect-free-zone can be identified.

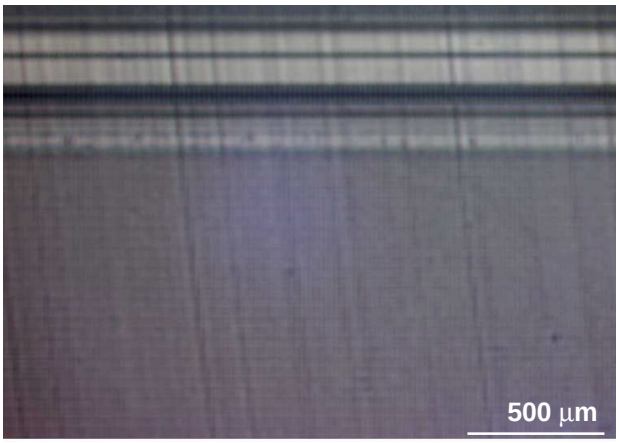

Figure 6. Picture after 12.5 min preferential etching, depth 20 µm.

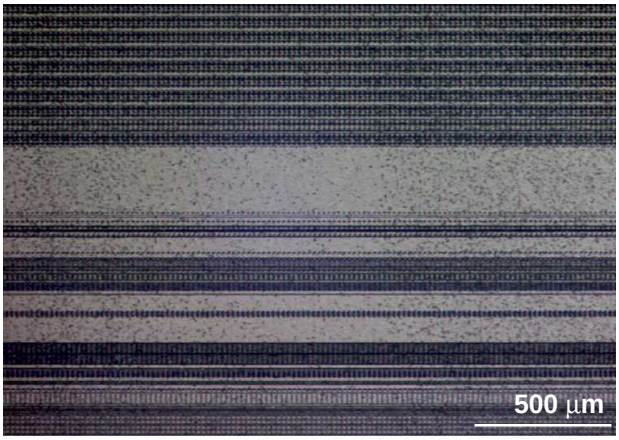

Figure 7. Picture after 22.5 min preferential etching, depth 50 µm.

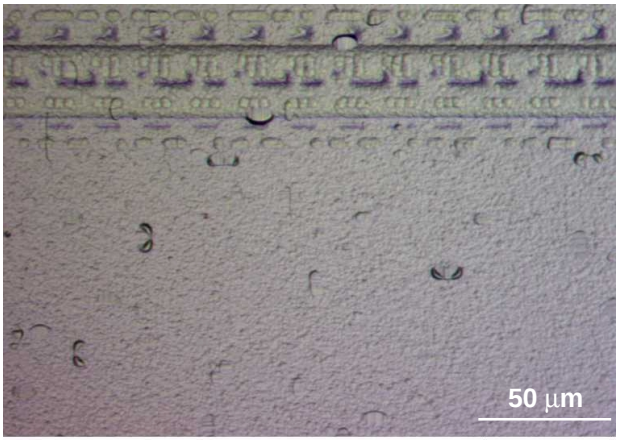

Figure 8. Close-up view of the defects seen in Fig 7.

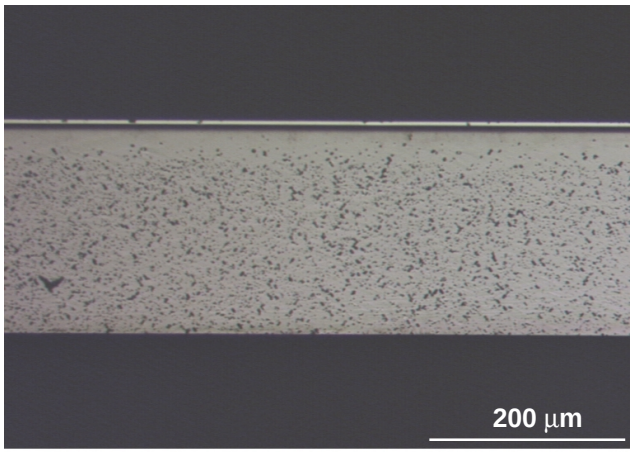

Figure 9. Cross-section of a processed CMOS wafer with internal gettering after preferential etching.

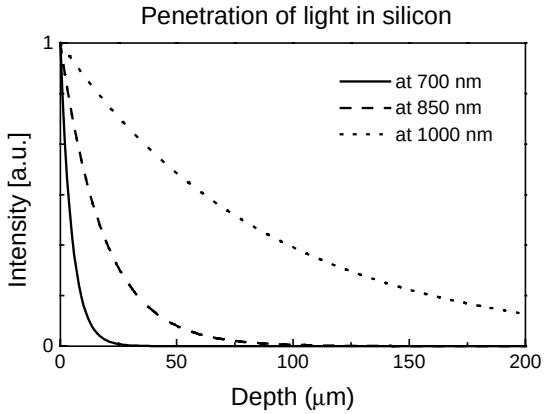

Figure 10. Penetration depths of light in silicon. Data from [6]

4. Discussion

The wavelength dependence indicates that the ring formed pattern seen in the images arise from the bulk of the wafer. In Fig. 10 a graph of the penetration of light into silicon is shown, and it is seen that at 700 nm the light reaches 25 μm in the wafer bulk, which is well below the epi-layer. The larger contrast difference, shown in Fig. 3, for longer wavelengths arise from a larger portion of carriers collected deeper in the bulk.

The results from the structural analysis points at two irregularities, both dopant striation and deeper lying oxygen induced stacking faults. Since the etch-rate of the Yang-etchant depends on the doping concentration the grooves in Fig. 6 is an indicator of striations in the doping concentration of the bulk material. Bulk recombination depends on the doping concentration, thus, rings of the sensitivity could also be explained this way. As seen in Fig. 10, 700 nm light penetrates to the depth where the dopant striations are located. The contrast of the stripes, however, is very low at this wavelength (see Fig. 3). Additionally, the spatial spread of the grooves seen in Fig 6, is much smaller than the effects that were seen when operating the chip, as shown in Fig. 4.

The stacking faults, as shown in Figs. 7-9, are often decorated with impurities creating recombination or generation centers. A recombination center would result in brighter stripes in areas of less defects, due to the smaller recombination. In Fig. 7, the area with a smaller density of defects have a spread of about 500-800 μm.

Depending on where on a sensor this pattern is located it is possible that observed structural defects correlates to brighter stripes as those seen in Fig. 4. In addition, it is shown in Fig. 9 that the increased defect concentration starts below 20 μm deep in the wafer and this correlates well to the wavelength dependence.

5. Conclusion

Collecting the results from wavelength dependence, the defect depth and the spatial resolution it is concluded that the most likely cause of the observed ring pattern in the images of the CMOS camera chips is crystal defects induced by oxygen precipitation.

6. References

[1] Y. Hiroshima, S. Matsumoto, T. Kuriyama and T. Kuroda, " CCD Image Sensors Fabricated on Epi-Wafers" *Electronics and Communications in Japan*, Vol. 67-C, pp. 1004-1011, 1984.

[2] Y. Murakami, Y. Satoh, H. Furuya and T. Shingyouji, "Effects of oxygen-related defects on the leakage current of silicon p/n junctions", *J Appl. Phys*. Vol. 84, pp. 3175-3186, 1998.

[3] L. Jastrzebski, R. Saydan, H. Elabd, W. Henry and E. Savoye, "The Effect of Heavy Metal Contamination on Defects in CCD Images", *J. Electrochem. Soc*., Vol. 137, pp. 242-248, 1990.

[4] J. A Gregory, B. E. Burke, M. J. Cooper, R. W. Mountain and B.B. Kosicki, "Fabrication of large-area CCD detectors on high-purity, float-zone silicon", *Nucl. Instr. Meth. A*, Vol. 377, pp 325-333, 1996.

[5] K. H. Yang, *J. Electrochem. Soc*. Vol. 131, p. 1140, 1984.

[6] *Properties of silicon,* (EMIS datareviews series, No 4), Inspec/IEE, ISBN; 0852964757, London, 1988.